Title: Coordinated IL-2 and TGF-β Signaling Activates Stable Regulatory T Cells and Promotes Immune Tolerance

One Sentence Summary

CUE-401 coordinates IL-2 and TGF-β signaling to expand and activate regulatory T cells and restrain autoimmune responses.

Authors

Nicholas M. Jackson[1], Javier A. Carrero[1], Kristin Yeung[2], Evelyn Needham[2], Emily Christie[2], Natalie Yakobian[1], Challen Pretorius[1], Stella Hoft[1], Kirsten Foley[1], Eric Ford[1], Simon Low[2], Ronald Seidel[2], Anish Suri[2], Natasha M. Girgis[2], Steven N. Quayle[2], Richard J. DiPaolo[1*]

[1]Department of Molecular Microbiology and Immunology, Saint Louis University School of Medicine, Saint Louis, Missouri

[2]CUE Biopharma, Boston, Massachusetts

Corresponding author, richard.dipaolo@health.slu.edu

Abstract

Establishing immune tolerance requires the integration of cytokine signals that favor regulatory T cell (Treg) function over effector differentiation, yet how such coordination can be achieved selectively in vivo remains incompletely defined. Regulatory T cells are essential for maintaining immune homeostasis and peripheral tolerance, and both interleukin-2 (IL-2) and transforming growth factor–β (TGF-β) contribute to Treg activation, differentiation, and stability in a highly context-dependent manner. Here, we examine the consequences of coordinated IL-2 and TGF-β3 signaling using an engineered cytokine construct combining attenuated IL-2 with receptor-masked TGF-β3. In vitro, attenuated IL-2/TGF-β3 signaling promoted conversion of naïve $CD4^+$ T cells into $Foxp3^+$ induced Tregs, expanded endogenous Tregs, and suppressed inflammatory cytokine production by memory and effector $CD4^+$ T cells. In vivo, a

single administration selectively increased the frequency of $CD4^+Foxp3^+$ regulatory T cells exhibiting an activated and stable phenotype, while minimally activating $Foxp3^-$ conventional $CD4^+$ T cells relative to IL-2 alone. In a Treg-deficiency–driven adoptive transfer model of autoimmunity, early exposure to coordinated IL-2/TGF-β3 signaling enhanced Treg activation, reduced tissue infiltration by autoreactive T cells, and conferred sustained protection from autoimmune gastritis in the absence of continued treatment. Together, these findings identify a mode of coordinated IL-2 and TGF-β3 signaling sufficient to stabilize regulatory T cell responses and promote immune tolerance while limiting activation of conventional $CD4^+$ T cells, highlighting signal integration as a determinant of tolerogenic immune regulation in vivo.

Introduction

Autoimmune diseases arise from the breakdown of peripheral immune tolerance, resulting in persistent immune-mediated damage to self-tissues. The discovery of $CD4^+CD25^+$ regulatory T cells (Tregs) marked a paradigm shift in understanding immune tolerance (*1*). Tregs maintain tolerance by suppressing autoreactive effector T cell responses while preserving protective immunity through multiple mechanisms, including consumption of interleukin-2 (IL-2), expression of inhibitory receptors (e.g. CTLA-4), and production of immunoregulatory cytokines, such as transforming growth factor–β (TGF-β) (*2*). The essential role of Tregs in immune homeostasis is underscored by the severe autoimmune pathology observed in humans and mice with mutations in the transcription factor Foxp3, which is required for Treg lineage commitment and stability (*3-6*).

Tregs are classically defined by expression of CD4, the high-affinity IL-2 receptor α-chain (CD25), and Foxp3. This population includes thymus-derived natural Tregs (nTregs) and peripherally induced Tregs (pTregs), which arise from conventional $CD4^+$ T cells in response to antigenic stimulation and cytokine cues (*7, 8*). In vitro, naïve $CD4^+$ T cells stimulated with TCR signals plus TGF-β, and IL-2 differentiate into $Foxp3^+$ induced Tregs (iTregs) with potent suppressive activity (*9*). Precise modulation of IL-2–

51 dependent STAT5 activation together with TGF-β–mediated Foxp3 induction is also critical for
52 maintaining stable, suppressive Tregs (*9-11*). Accordingly, this cytokine combination has been widely
53 used to generate suppressive iTregs ex vivo for adoptive cell therapies that are effective in preclinical
54 models of autoimmunity and graft-versus-host disease (*12-14*).
55
56 The immunosuppressive capacity of Tregs has motivated their therapeutic use in transplantation and
57 immune-mediated diseases. Several different IL-2 variants (muteins) have been engineered to activate and
58 expand Tregs and are being tested for effectiveness in treating inflammatory diseases (*15-17*). Key
59 challenges include a limited therapeutic window due to off-target stimulation of non-Treg populations, the
60 short half-life of IL-2, and the need for precise dosing to achieve selective Treg engagement. Moreover,
61 Treg induction, stability, and specialization in vivo often require additional cues, including TGF-β.
62 Coordinating IL-2 and TGF-β signaling in vivo is challenging due to short in vivo half-lives of cytokines,
63 tolerability considerations, and the need to co-engage receptors on the same target cell(s). CUE-401, a
64 novel Fc-based IL-2/TGF-β3 fusion protein designed for coordinated delivery of IL-2 and TGF-β3 signals
65 in vivo, was designed to address these challenges. CUE-401 includes an attenuated IL-2 mutein (F42A,
66 H16A) with reduced affinity for CD25 and CD122 (*18-20*), and a novel receptor-masked attenuated TGF-
67 β3 variant, linked via flexible linkers to an Fc scaffold to promote IL-2/TGF-β3 co-signaling and extend
68 half-life. All amino acid sequences are human-derived, and both cytokines cross-react with mouse
69 receptors (*21, 22*). Here, we evaluated the biological activities of CUE-401 in vitro and in vivo for its
70 ability to enhance Tregs, suppress effector T cell responses, and mitigate autoimmune pathology.
71
72 **Results**
73
74 **CUE-401 delivers IL-2 and TGF-β signals to T cells**
75 CUE-401 is a bispecific fusion protein composed of affinity attenuated variants of IL-2 and TGF-β3 (Fig.
76 1A). The IL-2 mutein (F42A and H16A) reduces affinity to IL-2Rα (CD25) and IL-2Rβ (CD122) (*18*). The

77 TGF-β3 component is engineered as a monomeric, receptor masked variant to attenuate receptor affinity.
78 The TGF-β3 moiety carries a C77S mutation that prevents formation of the interchain disulfide bond while
79 maintaining its ability to assemble the natural signaling complex. Masking of the TGF-β3 moiety is
80 achieved through fusion to a modified TGF-β receptor II extracellular domain lacking the N-terminal
81 residues required for productive association with TGF-β receptor I and containing a D118A substitution
82 that reduces affinity for TGF-β3 relative to the wild-type receptor (*23, 24*). This configuration limits
83 constitutive TGF-β receptor engagement while permitting biological activity upon cell-associated
84 presentation. The IL-2 and TGF-β3 domains are connected via flexible linkers to a heterodimeric Fc
85 scaffold to support coordinated signaling and molecular stability.
86
87 To quantify IL-2 activity, CTLL-2 proliferation assays were performed comparing wild-type human IL-2
88 (Proleukin), CUE-401, and a construct containing the attenuated IL-2 moiety lacking the TGF-β3 domain
89 (CUE-401ΔTGFβ; Fig. 1B). Both CUE-401 and CUE-401ΔTGFβ induced dose-dependent proliferation
90 that was reduced compared to Proleukin, consistent with attenuated IL-2 receptor signaling (Fig. 1B). TGF-
91 β3 signaling activity was assessed by SMAD2/3 phosphorylation in murine splenocytes. CUE-401 induced
92 robust phosphorylation of SMAD2/3 comparable to recombinant TGF-β3, whereas recombinant IL-2 alone
93 failed to do so. SMAD2/3 phosphorylation induced by CUE-401 was abrogated by pretreatment with the
94 selective TGF-β receptor inhibitor SB431542, confirming engagement of canonical TGF-β receptor
95 signaling pathways (Fig. 1C).
96
97 **CUE-401 induces and expands Tregs and suppresses effector T cell function in vitro**
98 Having established that both cytokine components of the engineered construct were biologically active, we
99 next examined whether coordinated IL-2 and TGF-β3 attenuated signaling could induce de novo Foxp3
100 expression in $CD4^+$ T cells. $CD4^+CD8^-$Foxp3.GFP^- thymic T cells were sorted from thymi of
101 BALB/c.Foxp3.eGFP mice and stimulated with anti-CD3/anti-CD28 in the presence of recombinant human
102 IL-2 (rhIL-2), rhIL-2 plus recombinant human TGF-β3 (rhTGF-β3), or the engineered IL-2/TGF-β3

103 construct (Fig. 2). Stimulation with IL-2 alone induced minimal Foxp3 expression (~1%), whereas
104 combined IL-2 and TGF-β3 signaling, delivered either as separate recombinant cytokines or engineered
105 attenuated IL-2/TGF-β-Fc configuration, induced Foxp3 expression in more than 75% of $CD4^+$ T cells (Fig.
106 2A). Foxp3 induction occurred in a dose-dependent manner, with an EC_{50} of ~18 nM (Fig. 2B). These
107 findings indicate that coordinated and attenuated IL-2/TGF-β3 signaling is sufficient to drive inducible
108 regulatory T cell (iTreg) differentiation from naïve $CD4^+$ T cells.
109
110 To assess whether CUE-401 expands endogenous $CD4^+Foxp3^+$ Tregs, $CD4^+Foxp3.eGFP^+$ Tregs sorted
111 from the spleens of BALB/c.Foxp3.eGFP mice were stimulated with anti-CD3/anti-CD28 in the presence
112 of presence of either rhIL-2 alone or the engineered IL-2/TGF-β3 construct. As expected, Tregs maintained
113 Foxp3 expression when cultured with rhIL-2 (Fig. 2C). Similarly, Tregs stimulated in the presence of CUE-
114 401 maintained Foxp3 expression and expanded in a dose-dependent manner (Fig. 2D), indicating that this
115 signaling configuration supports both lineage stability and proliferative capacity of mature Tregs.
116
117 To determine the effects of coordinated signaling of the attenuated IL-2/TGF-β3 influences
118 effector/memory T cells, $CD4^+CD44^{hi}Foxp3.eGFP^-$ cells sorted from spleens of BALB/c.Foxp3.eGFP mice
119 were stimulated with anti-CD3/anti-CD28 in the presence of either rhIL-2, rhIL-2 + rhTGF-β3, or CUE-
120 401 (Fig. 2E). Treatment with rhIL-2 resulted in minimal induction of Foxp3 expression (~1%). However,
121 stimulation of these purified effector/memory T cells in the presence of rhIL-2 + rhTGF-β3 or CUE-401
122 induced Foxp3 expression in ~10% of effector/memory $CD4^+$ T cells (Fig. 2E-F). We further assessed
123 cytokine production by effector/memory $CD4^+$ T cells under these conditions. Stimulation in the presence
124 of IL-2 alone resulted in robust secretion of IFN-γ, IL-4, TNF, and IL-17A. In contrast, coordinated
125 IL-2/TGF-β signaling markedly reduced secretion of IFN-γ, IL-4, and TNF relative to IL-2 alone (Fig. 2G),
126 indicating suppression of pro-inflammatory effector function.
127 Collectively, these results define three distinct immunological outcomes of the coordinated signaling by
128 attenuated the IL-2 and TGF-β signaling in vitro: induction of $Foxp3^+$ regulatory T cells from naïve $CD4^+$

129 T cell precursors, maintenance and expansion of endogenous regulatory T cells, and partial reprogramming
130 of effector/memory $CD4^+$ T cells toward a less inflammatory state.
131

132 **Administration of coordinated IL-2/TGF-β induces robust expansion of stable regulatory T cells in**
133 **mice**

134 To assess the in vivo consequences of coordinated signaling by attenuated IL-2 and TGF-β, BALB/c mice
135 received a single administration of the engineered cytokine construct or vehicle control (PBS). Six days
136 after treatment, the frequency of $CD4^+Foxp3^+$ regulatory T cells in the spleen increased to approximately
137 61% of the $CD4^+$ T cell compartment in treated animals, compared with approximately 20% in control mice
138 (Fig. 3A-B). To determine whether regulatory T cells expanded under these conditions exhibited features
139 of lineage stability, we analyzed methylation of the Treg-specific demethylated region (TSDR), a CpG-rich
140 enhancer element within the Foxp3 locus (CNS2) associated with stable Foxp3 expression (*25*).
141 Splenocytes from vehicle-treated and cytokine-treated mice were sorted into $CD4^+Foxp3.eGFP^+$ and
142 $CD4^+Foxp3.eGFP^-$ populations (Fig. 3C). Regulatory T cells from treated mice displayed a degree of TSDR
143 demethylation comparable to that observed in endogenous regulatory T cells from control animals, whereas
144 conventional $CD4^+Foxp3^-$ T cells from treated mice retained a methylation profile indistinguishable from
145 that of control conventional T cells (Fig. 3D). Consistent with these epigenetic features, regulatory T cells
146 isolated from both treated and control mice maintained Foxp3 expression following ex vivo restimulation
147 for six days in the absence of continued cytokine exposure (Fig. 3E). Together, these findings indicate that
148 coordinated the IL-2 and TGF-β signaling provided by CUE-401 selectively expands regulatory T cells in
149 vivo while preserving epigenetic and transcriptional features associated with stable lineage commitment.
150

151 **Expanded regulatory T cells exhibit an activated phenotype following combined IL-2/TGF-β**
152 **administration**

153 Having established that coordinated IL-2 and TGF-β3 signaling induces robust expansion of regulatory T
154 cells in vivo, we next examined the phenotypic characteristics of regulatory T cells six days following
155 treatment. Consistent with earlier observations, treatment resulted in a marked increase in the frequency of
156 $CD4^{+}Foxp3^{+}$ regulatory T cells relative to vehicle-treated controls (Fig. 4A). We therefore assessed
157 expression of surface and intracellular markers associated with regulatory T cell activation and suppressive
158 function, including Foxp3, GITR, CD25, CTLA-4, CD103, CD73, CD38, CD134, CD137, and Ki67 (*26,*
159 *27*). Multidimensional flow cytometry analysis followed by UMAP projection revealed enrichment of
160 regulatory T cell clusters exhibiting features of activation in treated mice, including increased frequencies
161 of $GITR^{hi}/CD25^{hi}$ and $CTLA\text{-}4^{hi}/CD103^{hi}$ Tregs, and higher expression of CD25, CTLA-4, and GITR
162 overall (Fig. 4A–C). At the population level, regulatory T cells from treated animals displayed increased
163 expression of CD25, CTLA-4, and GITR, consistent with enhanced responsiveness to IL-2 and acquisition
164 of suppressive effector features (Fig. 4C).
165
166 To further characterize the transcriptional state of regulatory T cells expanded under coordinated
167 IL-2/TGF-β3 signaling, we performed bulk RNA sequencing on purified $CD4^{+}Foxp3^{+}$ T cells from treated
168 and control mice (Fig. 4D). Regulatory T cells from treated animals exhibited increased expression of genes
169 associated with regulatory T cell activation, tissue localization, and suppressive function, including *Itgae*
170 (CD103), *Nrp1*, *Il2ra*, *Il2rb*, *Lag3*, *Tnfrsf18* (GITR), *Icosl*, and *Klrg1* (*28-32*). Together, these phenotypic
171 and transcriptional analyses indicate that regulatory T cells expanded under coordinated IL-2 and TGF-β
172 signaling acquire an activated regulatory program associated with enhanced suppressive capacity,
173 complementing the observed epigenetic and transcriptional stability of the expanded population (*33-36*).
174
175 **Combined IL-2 and TGF-β signaling responses in Tregs are distinct from IL-2 alone**
176 To isolate the contribution of TGF-β signaling and distinguish the biological effects of coordinated
177 IL-2/TGF-β3 signaling from those of IL-2 alone, we compared the engineered IL-2/TGF-β3 construct
178 (CUE-401) with an otherwise identical IL-2–only variant lacking the TGF-β3 domain (CUE-401ΔTGF-

179 β3). Both constructs incorporate the same attenuated IL-2-Fc moiety, enabling direct comparison of IL-2
180 signaling in the presence or absence of concurrent TGF-β3 input. In vivo, administration of either construct
181 resulted in significant expansion of splenic regulatory T cells; however, regulatory T cell frequencies were
182 consistently higher following coordinated IL-2/TGF-β3 signaling (Fig. 5A, B). Moreover, regulatory T cells
183 expanded under coordinated IL-2/TGF-β3 signaling conditions exhibited a greater proportion of GITR^{hi}
184 CD38^{hi} Tregs compared with those expanded by IL-2 alone (Fig. 5C, D), consistent with acquisition of an
185 activated regulatory phenotype.
186
187 Notably, IL-2 signaling in the absence of TGF-β3 led to broader activation of conventional CD4^{+} T cells.
188 (Fig. 5E–F). Treatment with the IL-2–only construct increased expression of CD25 and CD103 on Foxp3^{-}
189 conventional CD4^{+} T cells, whereas coordinated IL-2/TGF-β3 signaling did not induce comparable
190 upregulation of these markers in the conventional T cell compartment (Fig. 5E–F), indicating enhanced
191 regulatory selectivity when TGF-β signaling is integrated with IL-2.
192
193 To further define differences in signaling outcomes at the transcriptional level, we performed RNA
194 sequencing on sorted CD4^{+}Foxp3.eGFP^{+} regulatory T cells and CD4^{+}Foxp3.eGFP^{-} conventional T cells
195 from mice treated with vehicle, IL-2 alone (CUE-401ΔTGF-β3), or coordinated IL-2/TGF-β3 signaling
196 (CUE-401). Both IL-2 alone and coordinated IL-2/TGF-β signaling increased expression of core regulatory
197 T cell–associated genes, including *Ctla4*, *Foxp3*, *Il2ra*, and *Lag3*, relative to vehicle-treated control (Fig.
198 5G). However, several transcripts induced in regulatory T cells by IL-2 alone were not comparably induced
199 when IL-2 signaling occurred in conjunction with TGF-β3, indicating qualitative differences in downstream
200 signaling programs. Conversely, coordinated IL-2/TGF-β3 signaling selectively induced a set of transcripts
201 previously associated with TGF-β–dependent regulation, including *Alpk1*, *Amot1*, *Cyp4f18*, *Lgmn*, and
202 *Trim47*, which were not induced by IL-2 alone. Together, these findings demonstrate that integrated IL-2
203 and TGF-β signaling establishes a regulatory T cell transcriptional state that is distinct from, and not merely
204 an amplification of, the program elicited by IL-2 in isolation.

205 In contrast, within the $CD4^+Foxp3^-$ conventional T cell compartment, IL-2 signaling in the absence of
206 concurrent TGF-β input elicited a transcriptional program characteristic of IL-2–driven cellular activation.
207 Treatment with the IL-2–only construct (CUE-401ΔTGF-β3) resulted in increased expression of genes
208 associated with effector differentiation and activation, including *Ccl4*, *Eomes*, *Fut7*, *Gzma*, *Gzmb*, *Lgals1*,
209 *Lgals3*, *Ly6a*, *Morrbid*, *Nfil3*, and *S100a6*. These transcripts were not comparably induced in conventional
210 $CD4^+$ T cells from mice receiving coordinated IL-2 and TGF-β3 signaling (CUE-401, Fig. 5H). Together,
211 these data indicate that IL-2 signaling alone promotes activation-associated transcriptional programs in
212 conventional $CD4^+$ T cells, whereas integration of TGF-β3 signaling constrains this response. Thus,
213 coordinated IL-2 and TGF-β3 signaling differentially regulates regulatory and conventional $CD4^+$ T cell
214 compartments, favoring regulatory T cell–specific activation while limiting IL-2–driven activation of
215 conventional T cells.
216
217 **Early coordinated IL-2 and TGF-β signaling suppresses autoreactive T cell responses and limits**
218 **autoimmune gastritis.**
219 To examine the consequences of coordinated IL-2 and TGF-β3 signaling in an established model of Treg
220 deficiency–driven autoimmunity, we employed a well-characterized murine model of autoimmune gastritis
221 in which $CD25^+$ regulatory T cells are depleted from BALB/c splenocytes prior to transfer into athymic
222 BALB/c *nu/nu* recipients (*1*). Depletion of regulatory T cells in this system reliably results in the
223 development of autoimmune gastritis in all recipients. To enable tracking of antigen-specific autoreactive
224 conventional $CD4^+$ T cells, a small number of $CD4^+$ TCR-transgenic T cells specific for the gastric
225 autoantigen H^+/K^+ ATPase and expressing the Thy1.1 congenic marker (*37*) were admixed with
226 CD25-depleted BALB/c splenocytes ($Thy1.2^+$) before transfer. A representative flow cytometric analysis
227 of the transferred $CD4^+$ T cell populations is shown in Fig. 6A.
228
229 Recipient BALB/c *nu/nu* mice were administered vehicle or CUE-401 on days 1 and 14 following transfer.
230 Sixty-two days after transfer, mice receiving CUE-401 exhibited a marked reduction in the frequency of

231 autoreactive H^+/K^+ ATPase-specific $CD4^+Thy1.1^+$ T cells infiltrating the gastric mucosa compared with
232 vehicle-treated controls (approximately 10% versus 44%, respectively; $P = 0.0005$; Fig. 6B–C).
233 Histopathological examination of stomach tissue was performed to assess disease severity, including
234 inflammation, glandular atrophy, and epithelial hyperplasia, hallmark features of autoimmune gastritis (*38*).
235 As expected, vehicle-treated mice developed moderate-to-severe autoimmune gastritis, with a median
236 disease score of 6 on a 12-point scale. In contrast, mice that received coordinated IL-2/TGF-β3 signaling
237 displayed significantly reduced pathology, with a median disease score of 3, and no detectable gastritis in
238 a subset of animals (Fig. 6D, E). Together, these findings indicate that early and transient exposure to
239 coordinated IL-2 and TGF-β3 signaling is sufficient to durably constrain autoreactive $CD4^+$ T cell
240 accumulation and limit tissue pathology in a stringent model of regulatory T cell deficiency–driven
241 autoimmunity.
242
243 **Coordinated IL-2 and TGF-β signaling induces a distinct regulatory T cell state in a disease context**
244 To investigate the immunological mechanisms underlying suppression of autoimmune gastritis following
245 coordinated IL-2 and TGF-β3 signaling, we analyzed immune populations from vehicle- and
246 cytokine-treated mice using flow cytometry and single-cell RNA sequencing. Cells were isolated from
247 gastric draining lymph nodes and spleens seven days after cell transfer, corresponding to six days following
248 a single administration of vehicle or coordinated IL-2/TGF-β3 signaling. At this time point, the frequency
249 of $CD4^+Foxp3^+$ regulatory T cells in gastric draining lymph nodes was significantly increased in treated
250 mice (~25%) compared with vehicle-treated controls (~10%, Fig. 7A, B). To further define regulatory T
251 cell phenotypes in this inflammatory setting, $CD4^+Foxp3^+$ T cells were subjected to high-dimensional flow
252 cytometric analysis, including markers associated with regulatory activation and proliferation (Foxp3,
253 GITR, CD25, CTLA-4, CD103, CD73, CD38, CD134, CD137, and Ki67). Unsupervised dimensionality
254 reduction using Uniform Manifold Approximation and Projection (UMAP) revealed distinct clustering of
255 regulatory T cells from vehicle-treated versus cytokine-treated mice, indicating divergent protein
256 expression profiles between groups (Fig. 7C). Notably, regulatory T cells from treated mice exhibited

257 higher expression of CD25 compared with those from vehicle-treated controls (Fig. 7D), consistent with
258 enhanced IL-2 responsiveness in the disease setting.
259
260 To further characterize regulatory T cell states at the transcriptional level, we performed single-cell RNA
261 sequencing of cells isolated from gastric lymph nodes and spleens at the same time point. Foxp3^{+} regulatory
262 T cells formed discrete clusters in each treatment condition (Fig. 7F). Downstream analysis of Foxp3^{+} cells
263 revealed that regulatory T cells from cytokine-treated mice were significantly enriched for transcripts
264 associated with IL-2/STAT5 signaling compared with regulatory T cells from vehicle-treated controls
265 (Fig. 7G).
266
267 Consistent with these findings, differential gene expression analysis highlighted increased expression of
268 genes associated with regulatory T cell activation, survival, and suppressive potential in treated mice,
269 including *Il2ra* (CD25), *Tnfrsf4* (OX40), *Tnfrsf9* (4-1BB), *Tnfsf11* (RANKL), *Il1rl1* (ST2), and *Bcl2l1*
270 (BCL-xL) (Fig. 7H). Together, these data indicate that coordinated IL-2 and TGF-β3 signaling in a disease
271 context not only expands regulatory T cell populations but also promotes a distinct transcriptional and
272 phenotypic state associated with enhanced activation and survival. These early changes in regulatory T cell
273 state provide mechanistic insight into how regulatory dominance is established in an inflammatory
274 environment and may contribute to subsequent long-term suppression of autoimmune pathology.
275
276 **Discussion**
277 Regulatory T cell–mediated immune tolerance emerges from the integration of multiple cytokine-derived
278 signals that collectively shape lineage stability, activation state, and functional dominance over effector
279 responses. Although interleukin-2 (IL-2) and transforming growth factor-β (TGF-β) have long been
280 recognized as essential contributors to regulatory T cell biology, how these pathways can be coordinated in
281 vivo to selectively promote regulatory outcomes while constraining conventional T cell activation has
282 remained incompletely defined. In this study, we demonstrate that constrained and coordinated delivery of

attenuated IL-2 and TGF-β signals is sufficient to induce, expand, and stabilize regulatory T cells across multiple cellular contexts, leading to durable suppression of autoreactive immune responses.

Prior studies established that inducible regulatory T cells generated ex vivo with IL-2 and TGF-β can suppress autoimmune pathology following adoptive transfer (*33-36, 39, 40*). However, these approaches require cell manufacturing and do not address whether coordinated cytokine delivery can be achieved pharmacologically in vivo. Our findings show that coordinated delivery of IL-2 and TGF-β3 signaling can recapitulate key features of regulatory T cell induction and activation directly in vivo while avoiding broad activation of conventional $CD4^+$ T cells. Notably, regulatory T cells exposed to coordinated signaling acquired an activated phenotype characterized by increased expression of suppressive and survival-associated receptors, whereas such activation was not observed in $Foxp3^-$ conventional T cells. This selective response was not reproduced by an IL-2–only variant, supporting the premise that integration of TGF-β3 signaling qualitatively reshapes IL-2 responsiveness in a Treg-biased manner. Further dissection of receptor-proximal signaling dynamics and cell-type–specific cytokine engagement will be required to refine this model (*41*).

At the molecular level, regulatory T cells expanded under coordinated IL-2/TGF-β3 signaling exhibited durable Foxp3 expression, demethylation of the Foxp3 Treg-specific demethylated region (TSDR), and stable maintenance of Foxp3, all features associated with lineage commitment. These properties are particularly notable given reports that inducible regulatory T cells can exhibit instability under inflammatory conditions (*42-45*). Although overall regulatory T cell frequencies returned toward baseline approximately two weeks after treatment, expanded cells retained a stable $Foxp3^+$ phenotype in both homeostatic and inflammatory settings, consistent with physiological regulation of the compartment rather than loss of lineage identity. Future lineage-tracing studies will be important to definitively distinguish contributions of de novo induction versus selective expansion in vivo.

309

310 Mechanistically, coordinated IL-2 and TGF-β signaling promoted activation of CD25/IL-2/STAT5–
311 associated pathways in regulatory T cells while limiting induction of effector-associated transcriptional
312 programs in conventional $CD4^+$ T cells. Comparative studies using a TGF-β–deficient IL-2 variant
313 demonstrated that TGF-β3 is required both for selective regulatory T cell activation and for constraining
314 off-target IL-2–driven responses in conventional T cells. These findings indicate that the integration of IL-2
315 and TGF-β signaling does not simply amplify IL-2 activity but instead establishes a qualitatively distinct
316 signaling state biased toward regulatory outcomes. Whether this effect reflects altered cytokine receptor
317 geometry, localized cytokine concentration, temporal coordination of signaling pathways, or cooperative
318 receptor engagement remains an important question for future mechanistic investigation.
319 The immunological relevance of this coordinated signaling logic was particularly evident in a stringent
320 model of regulatory T cell deficiency–driven autoimmunity. Early, transient exposure to coordinated IL-2
321 and TGF-β signaling suppressed accumulation of autoreactive T cells, reduced tissue pathology, and
322 promoted establishment of regulatory dominance that persisted long after cytokine exposure had ceased.
323 Single-cell transcriptional analysis further revealed that regulatory T cells expanded under these conditions
324 acquired a distinct activation program characterized by enhanced IL-2/STAT5 signaling, expression of
325 costimulatory receptors, and pro-survival genes in disease-associated lymphoid tissues, suggesting that
326 early regulatory reprogramming contributes to long-term immune control.
327 While this study demonstrates that coordinated IL-2 and TGF-β3 signaling can promote regulatory T cell
328 dominance without enforced receptor co-engagement or antigen targeting, recent work by Sun et al.
329 describes an alternative strategy in which IL-2 and helminth derived TGF-β mimic are conditionally
330 coupled through a cis-acting surrogate agonist to drive peripheral regulatory T cell differentiation in vivo
331 (*46*). Together, these studies define complementary mechanistic solutions by which IL-2 and TGF-β
332 signaling can be integrated in vivo, reinforcing the concept that qualitative features of signal integration,
333 rather than cytokine availability alone, govern regulatory T cell fate and function.

334 Collectively, our findings establish coordinated and attenuated IL-2 and TGF-β3 signaling as a flexible
335 immunological framework for regulating regulatory T cell responses in vivo. By demonstrating that signal
336 attenuation and integration can selectively promote stable, lineage-committed regulatory T cells while
337 limiting conventional T cell activation, this work provides insight into fundamental principles governing
338 immune tolerance. Evaluation in additional disease models and human systems will further clarify how
339 distinct modes of cytokine coordination can be leveraged to engage regulatory pathways across diverse
340 immune contexts.
341
342 **Materials and Methods**
343
344 **Study design**
345 The objective of this research was to define the activities of a new biologic that co-engages IL-2 and TGF-
346 β pathways on regulatory T cells. This was accomplished by experimentally testing the function of the
347 biologic, named CUE-401, in vitro and in vivo. In vitro, testing was performed to address the induction of
348 iTregs from naïve $CD4^+$ T cells, maintenance of Foxp3 expression and expansion of existing Tregs, and
349 induction of Foxp3 expression with reduced proinflammatory cytokine production in a subset of
350 effector/memory $CD4^+$ T cells. CUE-401 was also administered to mice. Expression of Foxp3 and other
351 activation related proteins were measured by flow cytometry and compared by uniform manifold
352 approximation and projection analysis. Stability of in vivo Tregs was assessed by measuring the
353 methylation state of CpG sites in the Treg specific demethylated region, and $Foxp3^+$ cells were restimulated
354 to verify maintenance of Foxp3 expression. CUE-401's ability to affect disease severity was measured
355 through tracking autoreactive T cells, pathological scores of disease in the stomachs of an established mouse
356 model of autoimmunity. Single cell RNA sequencing was done to address potential mechanisms of action
357 for disease.
358
359 **CUE-401 design and production**

360 CUE-401 was produced by transient transfection of ExpiCHO-S cells using the Gibco ExpiCHO Expression
361 System Max Titer Protocol. Each transfection is performed with two plasmids at a 1:1 molar ratio encoding
362 (1) IL2 mutein linked to human IgG1Fc (knob) linked to monomeric TGFß3 and (2) human IgG1Fc (hole)
363 linked to truncated TGFßR2, respectively. Upon harvest, conditioned media was loaded onto a mAb Select
364 SuRe protein A column using an AKTA Pure 25 system for affinity-based purification. After a 10-column
365 volume (cv) wash with 20mM HEPES pH 7.5 + 1M NaCl, CUE-401 was eluted using 50mM glycine pH
366 2.8 directly into 10% 1M Tris pH 9.0 neutralization solution. Eluant was pooled, concentrated and loaded
367 onto a HiLoad 26/600 Superdex 200 for final step purification by size exclusion chromatography in 1x PBS
368 pH 7.4. Main protein elution peak was collected, pooled, concentrated, filtered using a 2um syringe filter.
369 Protein concentration was measured by absorbance at 280nm (A_{280}) using a NanoDrop system. Protein
370 integrity, size, solution state, and purity were confirmed by liquid chromatography-mass spectrometry,
371 SDS-PAGE, and analytical size exclusion chromatography. Final purified protein was aliquoted and stored
372 at -80ºC until use.
373
374 **Mice**
375 Female BALB/c Thy1.1^{+} mice were bred in house and BALB/c *nu/nu* (4–8 wk old) were purchased from
376 the Charles River Laboratory and housed under specific pathogen-free conditions. TCR transgenic mice
377 were crossed with BALB/c Thy1.1/1.1 expressing mice as previously described (*37*). TCR Transgenic
378 Thy1.1/1.1 expressing mice that develop autoimmune gastritis were crossed with BALB/c Thy1.1/1.1
379 Foxp3.eGFP reporter mice (C.Cg-*Foxp3*^{tm2Tch}/J) to generate TCR transgenic Thy1.1/1.1 Foxp3.eGFP
380 reporter mice (*42*). All animals were maintained in the Department of Comparative Medicine, Saint Louis
381 University School of Medicine in accordance with institutional guidelines (Association for Assessment and
382 Accreditation of Laboratory Animal Care, International accreditation number 000656).
383
384 **CUE-401 Dosing**

385 CUE-401 was formulated in sterile PBS, pH 7.4. Mice received intraperitoneal (i.p.) injections of CUE-401
386 at 2 mg/kg (100 μg/mL; 10 mL/kg; typical injection volume ~0.2–0.3 mL per 20–30 g mouse) or PBS
387 (vehicle) on the indicated schedule. For the adoptive transfer model, dosing occurred on days +1 and +14
388 post-transfer. For pharmacodynamic studies of Treg expansion, a single dose was administered, and tissues
389 were analyzed on day 6.
390
391 **CTLL-2 proliferation assays**
392 CTLL-2 cells were cultured in RPMI 1640 medium (Thermo Fisher Scientific, Waltham, MA, USA)
393 supplemented with 10% heat-inactivated fetal bovine serum (Thermo Fisher Scientific, Waltham, MA,
394 USA) and were starved of IL-2 for 22–24 h by washing cells free of cytokine and incubating them at
395 1×10^5 cells/mL in IL-2–free medium at 37°C with 5% CO_2. Cell viability and morphology were assessed
396 before and after starvation via acridine orange/propidium iodide staining using a Cellaca MX automated
397 cell counter (Nexcelom Bioscience, Lawrence, MA, USA). On the day of assay, 5×10^3 viable CTLL-2
398 cells were seeded in 96-well tissue-culture-treated plates (Corning/Costar, Corning, NY, USA) in 100 μL
399 medium, with outer wells filled with DPBS (Thermo Fisher Scientific, Waltham, MA, USA) to minimize
400 edge effects. Test molecules and recombinant rhIL-2 were prepared at 2× concentration and added in 100
401 μL to achieve a final volume of 200 μL per well, with all conditions plated in triplicate. After 72 h
402 incubation at 37°C, cell viability was quantified using CellTiter-Glo® reagent (Promega, Madison, WI,
403 USA): plates were equilibrated to room temperature, 100 μL of suspension was transferred to white
404 flat-bottom 96-well assay plates (Corning/Costar, Corning, NY, USA), an equal volume of CellTiter-Glo
405 was added via reverse pipetting, plates were agitated and incubated for 10 min, and luminescence was
406 measured using a Synergy Neo2 multimode plate reader (BioTek Instruments, Winooski, VT, USA).
407
408 **pSMAD Detection**
409 Murine splenocytes and human PBMCs were used to evaluate pSMAD2 signaling in response to
410 CUE-401 stimulation and TGF-β pathway inhibition. Fresh spleens from BALB/c mice were processed

411 through a 0.7-µm strainer to obtain single-cell suspensions, followed by ACK lysis, washing in PBS, and
412 counting on a Cellaca MX automated cell counter. Cells were aliquoted at 5×10^7 per condition and rested
413 for 2 h at 37°C, with subsets pre-treated for 90 min with 10 µM TGF-β inhibitor. PBMCs were thawed
414 and washed similarly. Cells were treated for 30 min at 37°C with IL-2, TGF-β3, CUE-401, or
415 combinations thereof, and then washed and lysed with RIPA buffer (Thermo Fisher Scientific, Waltham,
416 MA, USA) supplemented with Halt Protease/Phosphatase Inhibitor Cocktail (Thermo Fisher Scientific,
417 Waltham, MA, USA). Lysates were homogenized by pipetting, clarified by centrifugation at 10,000 rpm
418 for 10 min at 4°C, and protein content was quantified using a BCA assay. Samples were mixed with LDS
419 loading buffer (Thermo Fisher Scientific, Waltham, MA, USA), heated, and resolved on Bolt 4–12%
420 Bis-Tris Plus polyacrylamide gels (Thermo Fisher Scientific, Waltham, MA, USA) alongside SeeBlue
421 Plus Prestained Standards (Thermo Fisher Scientific, Waltham, MA, USA). Following electrophoresis,
422 proteins were transferred to PVDF membranes using the iBlot 2 Dry Blotting System (Thermo Fisher
423 Scientific, Waltham, MA, USA), then blocked for 2 h at room temperature in SuperBlock buffer (Thermo
424 Fisher Scientific, Waltham, MA, USA). Membranes were incubated overnight at 4°C with primary
425 monoclonal antibodies against phospho-SMAD2 (Cell Signaling Technology, Danvers, MA, USA) or
426 total SMAD2/3 (Cell Signaling Technology, Danvers, MA, USA). After washing, membranes were
427 incubated with HRP-conjugated goat anti-rabbit IgG (Cell Signaling Technology, Danvers, MA, USA)
428 for 1 h at room temperature, washed again, and developed using SuperSignal West Femto or West Pico
429 chemiluminescent substrates (Thermo Fisher Scientific, Waltham, MA, USA). Western blots were
430 imaged using a Syngene G:BOX darkroom imaging system (Syngene, Frederick, MD, USA). Band
431 intensities were analyzed to quantify pSMAD2 induction and inhibition across treatment conditions.
432

433 **Isolation of Immune Cells**

434 Isolation of immune cells from stomach tissue has been described previously (*38, 43*). Briefly, stomachs
435 were harvested from mice, gastric lymph nodes were removed, and the stomachs were dissected along the
436 lesser curvature. Stomachs were rinsed with cold PBS then injected with 10 mL of cold MACS buffer (1 x

437 PBS,0.5% BSA (Fisher Scientific Waltham, MA), 2 mM EDTA (Promega, Fitchburg, Wisconsin)) using a
438 27-gauge needle, to inflate the tissue and free infiltrating immune cells. After injection, the stomach was
439 diced and collected with the 10mL of MACS buffer and transferred to a 50 mL conical tube. The dispersed
440 stomach tissue was mixed thoroughly then passed through a 40-micron filter, washed with 40 mL of MACS
441 buffer and used for analysis. Immune cells from the spleen and gastric/pancreatic lymph node were
442 processed by dispersing on a 40-micron filter and washed with 15 mL of MACS buffer. Spleen cells were
443 spun down at 2000 RPM for 5 minutes after initial processing. Spleen cells were resuspended in 5 mL of
444 1x ACK lysis buffer (Thermo Fisher Scientific, Waltham, MA) for 10 seconds then washed with 45 mL of
445 MACS buffer and spun again at 2000 RPM for 5 minutes. Cells were resuspended and filtered again through
446 a 40-micron filter before being counted and utilized for experiments.
447
448 **T cell purification, iTreg differentiation, and nTreg expansion**
449 Inducible Tregs (iTreg) were generated as previously described (*9*). Briefly, $CD4^{+}CD8^{-}$ thymocytes or
450 $CD4^{+}$Foxp3.eGFP^{+} splenocytes were sorted from 6-8-wk-old BALB/c mice and stimulated with plate-
451 bound anti-CD3 (1 mg/ml) and anti-CD28 (2 mg/ml; BD Biosciences) in 24-well plates ($2.5x10^{5}$ cells/well)
452 in 2 ml RPMI media (modified RPMI 1640 (Corning, Tewksbury, Massachusetts) supplemented with 10%
453 fetal bovine serum (FBS; Biotechne, Minneapolis, Minnesota), 2 mM glutamine (Sigma-Aldrich), 100 U/ml
454 penicillin,100 mg/ml streptomycin (Sigma-Aldrich), 10 mM HEPES (Sigma-Aldrich), β-mercaptoethanol
455 (55mM), 1 mM essential amino acids (Gibco, Billings, Montana), and 1 mM sodium pyruvate (Sigma-
456 Aldrich) supplemented with recombinant human IL-2(rhIL-2) (National Institutes of Health, Bethesda,
457 Maryland) (100 U/ml). Recombinant human TGF-β3 (rhTGF-β3) (Biotechne) (5 ng/ml) was added to
458 induce iTregs. Cells were removed from plate-bound antibodies after 48 hours and added to new wells with
459 fresh media supplemented with 100 U/ml recombinant human IL-2. Cells were used after 7 days in culture.
460 Endogenous Treg expansion was assessed by isolating FACS-purified splenic $CD4^{+}$Foxp3.eGFP^{+} Tregs.
461 Tregs were stimulated with plate-bound anti-CD3 & anti-CD28 and expanded with IL-2 (100 U/mL) or
462 CUE-401 as indicated for 5–7 days. Foxp3 maintenance and cell counts were assessed by flow cytometry.

463

464 **Effector/Memory CD4$^+$ T-Cell Restimulation and Cytokine Quantification**

465 Splenic CD4$^+$CD44^{hi} Foxp3.eGFP$^-$ T cells were FACS-sorted and stimulated with plate-bound anti-CD3 &
466 anti-CD28 in the presence of rhIL-2 (100 U/mL), rhIL-2 + rhTGF-β3 (5 ng/mL), or CUE-401. For cytokine
467 secretion, cells were cultured at 1×10^6 cells/mL and restimulated with 25ng/mL phorbol myristate acetate
468 (PMA) (Sigma-Aldrich, St. Louis, Missouri), and 500 ng/mL ionomycin (Sigma-Aldrich), for 72 hours at
469 37°C for 72 h. Supernatants were collected and cytokine secretion was analyzed using a Th1, Th2, Th17
470 and IL-13 flex set (BD Biosciences) cytometric bead array kit and analyzed by flow cytometry following
471 the kit protocol and analyzed by flow cytometry.

472

473 **Treg Stability: TSDR (CNS2) Methylation Analysis**

474 CD4$^+$Foxp3$^+$ and CD4$^+$Foxp3$^-$ cells were sorted from spleens of PBS- or CUE-401-treated mice 6 days
475 post-dose. Genomic DNA was isolated (DNeasy Blood & Tissue Kit, Qiagen), bisulfite-converted (EZ
476 DNA Methylation-Gold Kit, Zymo Research), and the Foxp3 TSDR (CNS2) region was PCR-amplified
477 using validated primers spanning CpG sites within the enhancer. Amplicons were analyzed by
478 pyrosequencing [or Sanger sequencing of cloned products] to quantify methylation at individual CpGs.
479 Percent demethylation was calculated per CpG and averaged across the TSDR. Males and female mice
480 were used for TSDR analyses. Methylation state was normalized in female mice to account for the X-linked
481 Foxp3 locus inactivation in females.

482

483 **Bulk RNA-seq (Tregs and Tconv)**

484 CD4$^+$Foxp3.eGFP$^+$ regulatory T cells (Tregs) and CD4$^+$Foxp3.eGFP$^-$ conventional T cells (Tconv) were
485 FACS-sorted from spleens of PBS-, CUE-401–, or CUE-401ΔTGF-β3–treated BALB/c mice 6 days after
486 treatment (≥95% purity). Sorted cells were pelleted and immediately lysed in lysis buffer supplied with the
487 PureLink™ RNA Micro Kit (Invitrogen, Thermo Fisher Scientific), and total RNA was extracted according
488 to the manufacturer's protocol. RNA was eluted in RNase-free water and quantified using a Qubit RNA HS

489 Assay (Thermo Fisher). RNA integrity was assessed using the Agilent Bioanalyzer RNA Pico Kit, and only
490 samples with RIN ≥7.0 were used for library preparation.
491 Libraries were generated using the Takara-Clontech SMARTer construction method for Illumina with
492 poly-A mRNA enrichment, following manufacturer instructions. Indexed libraries were pooled and
493 sequenced on an Illumina NovaSeq x Pluse (300 cycles) platform (paired-end 2×100 bp), targeting ≥30
494 million read pairs per sample.
495 Samples were processed and sequenced at the Genome Technology Access Center @ McDonnell Genome
496 Institute in St. Louis, Missouri. RNA-seq reads were then aligned to the Ensembl GRCm39.113 primary
497 assembly with STAR version 2.7.11b. Gene counts were derived from the number of uniquely aligned
498 fragments by Subread:featureCount version 2.0.8. Differential gene expression analysis was performed
499 with EdgeR using quasi-likelihood F-test and was adjusted using the Benjamini-Hochberg method. Genes
500 with a false discovery rate (FDR) < 0.05 were considered significantly differentially expressed and adjusted
501 *P* value was $p < 0.05$. Level counts were obtained with featureCount. Visualization of the heatmaps was
502 generated using the R package pheatmap. Level counts were obtained with featureCounts. Differential gene
503 expression analyses were performed using DESeq2. Significance thresholds were set at an adjusted
504

505 **Cell purification and injection for adoptive transfer model of autoimmune gastritis**

506 Naive TxA23 T cells were isolated from a single-cell suspension of thymii from TxA23.Thy-1.1
507 Foxp3.eGFP mice. Thymocytes were lysed with ACK lysis buffer (BioSource) and washed with MACS
508 buffer prior to staining with CD4 BV421 (BD Biosciences) and CD8 PE (BD Biosciences). Cells were
509 placed in FACS sort buffer (2% FBS (Biotechne, Minneapolis, Minnesota), 100 U/ml penicillin, 100 mg/ml
510 streptomycin, in complete RPMI without phenol red (Sigma-Aldrich), and then purified using the BD
511 FACSAria Fusion cell sorter (BD Biosciences) to obtain $CD4^{+}CD8^{-}$ GFP^{-} Cells. BALB/c Splenocytes were
512 from spleens of healthy Thy-1.2 expressing BALB/c mice, RBC were removed with ACK lysis buffer and
513 then purified as follows. To deplete $CD25^{+}$ cells, cells were incubated for 10 min with anti-CD25-PE
514 (PC61), washed in MACS buffer, and incubated for an additional 10 min with anti-PE MACS microbeads

515 (Miltenyi Biotec, Bergisch Gladbach) then subjected to autoMACS purification (Miltenyi Biotec). The
516 negative fraction was used as CD25-depleted spleen cells. A typical depletion resulted in <1% of the $CD4^+$
517 cells expressing CD25. Prior to injection, all cells were washed twice in PBS. Naive TxA23.Thy-1.1 T cells
518 that were isolated from thymus, were mixed into the BALB/c Thy1.2 splenocyte population such that an
519 i.p. injection of 0.3 ml/mouse resulted in the transfer of 100,000 TxA23.Thy-1.1 T cells and 20×10^6 spleen
520 cells. Mice were monitored weekly and euthanized at ~ day 62 for tissue analyses.
521
522 **Histopathology**
523 BALB/c *nu/nu* mice were euthanized 62 days after receiving an adoptive transfer of splenocytes and naïve
524 $CD4^+$ T cells from autoreactive mice. The stomach opened, washed with cold PBS, and fixed in 4% neutral
525 buffered formalin. Fixed tissues were embedded in paraffin, stained with hematoxylin and eosin (H&E) by
526 Saint Louis University Research Histology Facility (SLU ASBRH) and disease pathology was scored
527 similarly to previously published assessments (*38*). Briefly multiple pathological features, including
528 inflammation, glandular atrophy, and epithelial hyperplasia were graded on a scale of 1–4, depending on
529 the extent of mononuclear cell infiltration and parietal and chief cell destruction. All stomach sections were
530 scored blindly by at least two individuals. General descriptions for scores are as follows: 0, healthy tissue
531 with no abnormalities 0.5, scattered lymphocytes throughout submucosa and muscularis with one or two
532 small dense blankets of lymphocytes; 1, two to four small dense clusters of lymphocytes in the
533 submucosa/mucosa; 1.5, two or three areas with intermediate infiltration spanning one-third of mucosa; 2,
534 big nodules of lymphocytic accumulation spanning half to all of mucosa; 2.5, big nodules of lymphocytic
535 accumulation spanning half to all of mucosa beginning to show evidence of parietal and chief cell
536 destruction (<25%); 3.0, heavy lymphocytic infiltration throughout mucosa, parietal and chief cell loss (25–
537 75%), and replacement by foamy cells; and 4.0, total parietal and chief cell loss, no mucosal architecture,
538 and many foamy cells.
539
540 **Flow Cytometry**

541 Immune cells were isolated from gastric mucosa, gastric/pancreatic or inguinal lymph nodes, and spleens
542 following the protocol previously described and cell surface staining was performed according to standard
543 procedures (*38, 43*). Immune cell subsets and proteins expressed on Tregs were identified using the
544 following antibodies: CD4 BV421, CD8 BV510, CD90.2 BV786, CD4 BV711, CD38 BV711, CD137
545 BV650 CD152 (CTLA4), CD103 PE-Cy7, CD8 PE, CD19 PE (BD Biosciences, Franklin Lakes, New
546 Jersey), CD73 PE/Dazzle594, CD90.1, CD134 PerCP/Cyanine 5.5, Ki67 BV605 (BioLegend, San Diego,
547 California), CD25 APC-eFluor780, Foxp3 APC, CD62L eFlour450, CD44 APC-eFlour780 (Thermo
548 Fisher Scientific). Cells were washed with 200 uL of PBS and stained in only PBS at 4°C. Cells were
549 fixed and permeabilized using eBioscience Foxp3/Transcription Factor Staining Buffer Set (Thermo
550 Fisher Scientific). Cells were incubated overnight with the intracellular antibodies and then washed and
551 analyzed by flow cytometry. Flow cytometry was performed on a BD LSRII, a BD Fortessa (BD
552 Biosciences), or a Cytek Aurora (Cytek Biosciences, Fremont California), and analyzed using FlowJo
553 (FlowJo, Ashland, OR).
554
555 **Single-Cell RNA-seq**
556 Cells from gastric lymph nodes and spleens (day 7 post transfer; day 6 post-treatment) were prepared as
557 above, RBC depleted as needed and filtered through 40µm strainers. Viability (>85%) was confirmed by
558 trypan blue. Cells were loaded on a 10x Genomics Chromium Controller (10X Genomics, Pleasanton,
559 CA) targeting up to 10,000 cells per library using the Next GEM Single Cell 5′ Kit v2 (10x #1000263).
560 cDNA amplification and library prep followed manufacturer protocols. PCR reactions were conducted in
561 the T100 Thermal Cycler (BioRad, Hercules, CA). Libraries were QC'd on an Agilent 2100 Bioanalyzer
562 (Agilent, Santa Clara, CA) and sequenced on an Illumina NovaSeq 6000 (Illumina, San Diego, CA).
563 Raw data were processed through CellRanger 6.0.2 pipeline (10x Genomics). Conditional repeats were
564 combined using cellranger aggr. Analysis was conducted using Seurat. (*44*) Each dataset was filtered to
565 exclude cells with low gene expression (<500/cell), high gene counts (outliers), and high percent
566 mitochondrial transcript load (>10%/cell). Datasets were merged, normalized, scaled, and dimensionally

567 reduced. Layers were joined and clusters were generated using a resolution of 2. Cluster identities were
568 established by attaining distinguishing genes per cluster and relating them to known profiles for immune
569 cells present in spleen and gastric lymph nodes. T cells clusters were subset and pathway analysis was
570 conducted using the R package enrichR and the Msig database for transcripts. Gene ontology, pathway
571 enrichment, and signature analyses (e.g., IL2/STAT5 signaling) were conducted
572 using fgsea and enrichR with MSigDB gene sets. Visualization of feature plots was performed using the
573 ggplot2 package in combination with the scCustomize package. Heatmaps were generated using Seurat's
574 DoHeatMap function. Statistical analyses were performed in Prism 10.0.0 (GraphPad Software). *P* values
575 less than 0.05 were considered significant.
576
577 **Statistical Analysis**
578 In vitro data are expressed as means of individual determination ± SD. In vivo data are expressed as median
579 of individual determination ± 95% confidence interval. Statistical analysis was performed using GraphPad
580 Prism 10 (GraphPad Software, San Diego, CA). Dose titrations of CUE-401 on nTregs utilized Kruskal-
581 Wallis test. Cytokine analysis utilized Wilcoxon matched-pairs signed rank test. In vitro treatment
582 comparisons between rhIL-2, rhIL-2 + TGF-β, and CUE-401 utilized Ordinary one-way ANOVA with
583 Tukey's multiple comparisons test. Histopathology score significance was performed using the Mann–
584 Whitney *U* test. Differential expression analysis between CUE-401 and PBS treated Tregs in scRNA-seq
585 data was performed using the Wilcoxon rank-sum test implemented in Seurat. Differentially expressed
586 genes were identified using the FindMarkers function in the Seurat package with default statistical
587 parameters, a log fold-change threshold of 0.6, and a minimum expression fraction of 0.1. Genes with an
588 adjusted p-value < 0.05 were considered differentially expressed. For bulk RNA sequencing, P-values were
589 adjusted for multiple comparisons using the Benjamini–Hochberg method to control false discovery rate.
590
591
592

593

594

595

596

597 **Figures**:

598 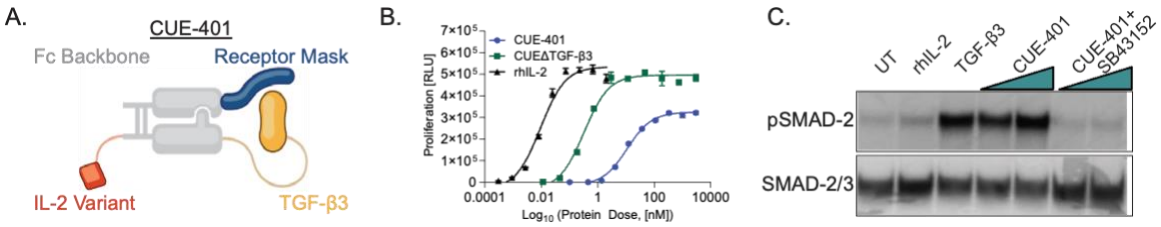

599 **Fig. 1. CUE-401 promotes IL-2 and TGF-β signaling activity.**

600 (**A**) Model of CUE-401 design. (**B**) CTLL-2 proliferation with recombinant human IL-2 (Proleukin),

601 CUE-401, or CUE-401ΔTGF-β3. (**C**) Immunoblot detecting phosphorylated SMAD-2 (pSMAD-2) and

602 total SMAD-2/3 after 30 minutes of stimulation with rhIL-2, rhTGF-β3, CUE-401, or CUE-401 +

603 SB43152.

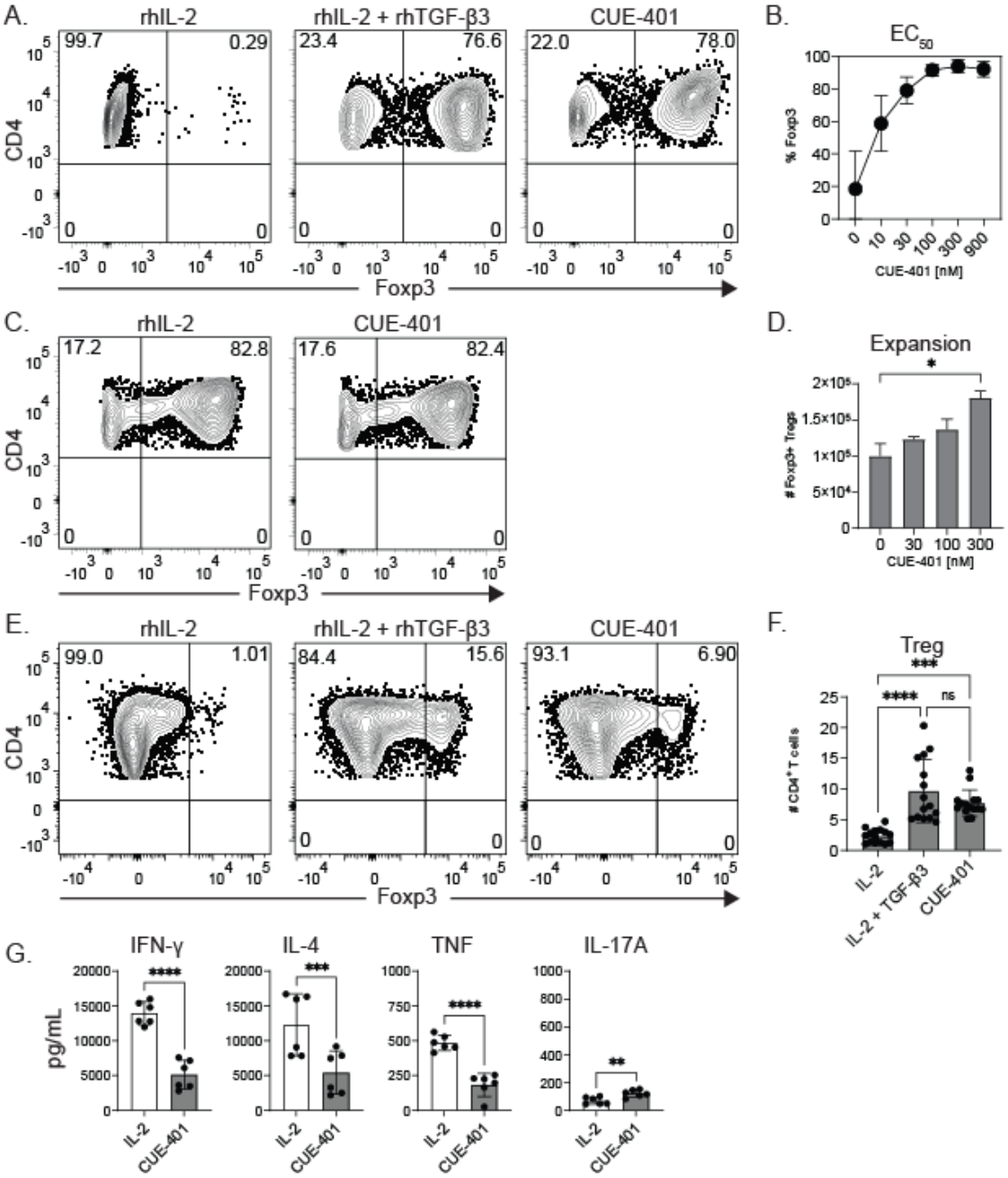

Fig. 2. CUE-401 promotes iTreg induction, nTreg expansion, and Teff suppression

(**A**). Representative flow cytometric analysis showing the percentage of $CD4^+$ gated cells expressing Foxp3 in vitro following stimulation with rhIL-2, rhIL-2 + rhTGF-β3, or CUE-401. (**B**). Dose-response curve displaying Foxp3 expression with increasing doses of CUE-401. (**C**). Representative flow cytometric analysis showing the percentage of $CD4^+$ gated cells expressing Foxp3 after six days in vitro

611 stimulation of Tregs with rhIL-2 or CUE-401. (**D**). Number of Foxp3 expressing cells at various
612 concentrations of CUE-401. (**E**). Flow cytometric analysis displaying the percentage of $CD4^+$ gated cells
613 expressing Foxp3 after six days in vitro simulation of Teff with rhIL-2, rhIL-2 + rhTGF-β3, or CUE-401.
614 (**F**) Percentages of $CD4^+Foxp3^+$ Tregs in rhIL-2, rhIL-2 + rhTGF-β3 and CUE-401 treated samples. (**G**).
615 Amounts of IFN-γ, IL-4, TNF, and IL-17A secreted from $CD4^+CD44^{hi}$ Foxp3.GFP^- T cells with rhIL-2 or
616 CUE-401 treatment. Flow cytometry plots are representative of individual sorted samples analyzed from
617 thymus (A) or spleen (D,F,G) of 4-8 healthy BALB/c mice. EC_{50} calculated by taking the concentration
618 halfway between the top and bottom value (approximately 20-80%). Bars in each graph represent the
619 mean +/-SD. *P*-values calculated using Kruskal-Wallis test (D), ordinary one-way ANOVA with Tukey's
620 multiple comparisons test (F), or Wilcoxon matched-pairs signed rank test (G) with $*p = 0.0332$, $**p =$
621 0.0021, $***p = 0.0002$, and $****p < 0.0001$.
622
623

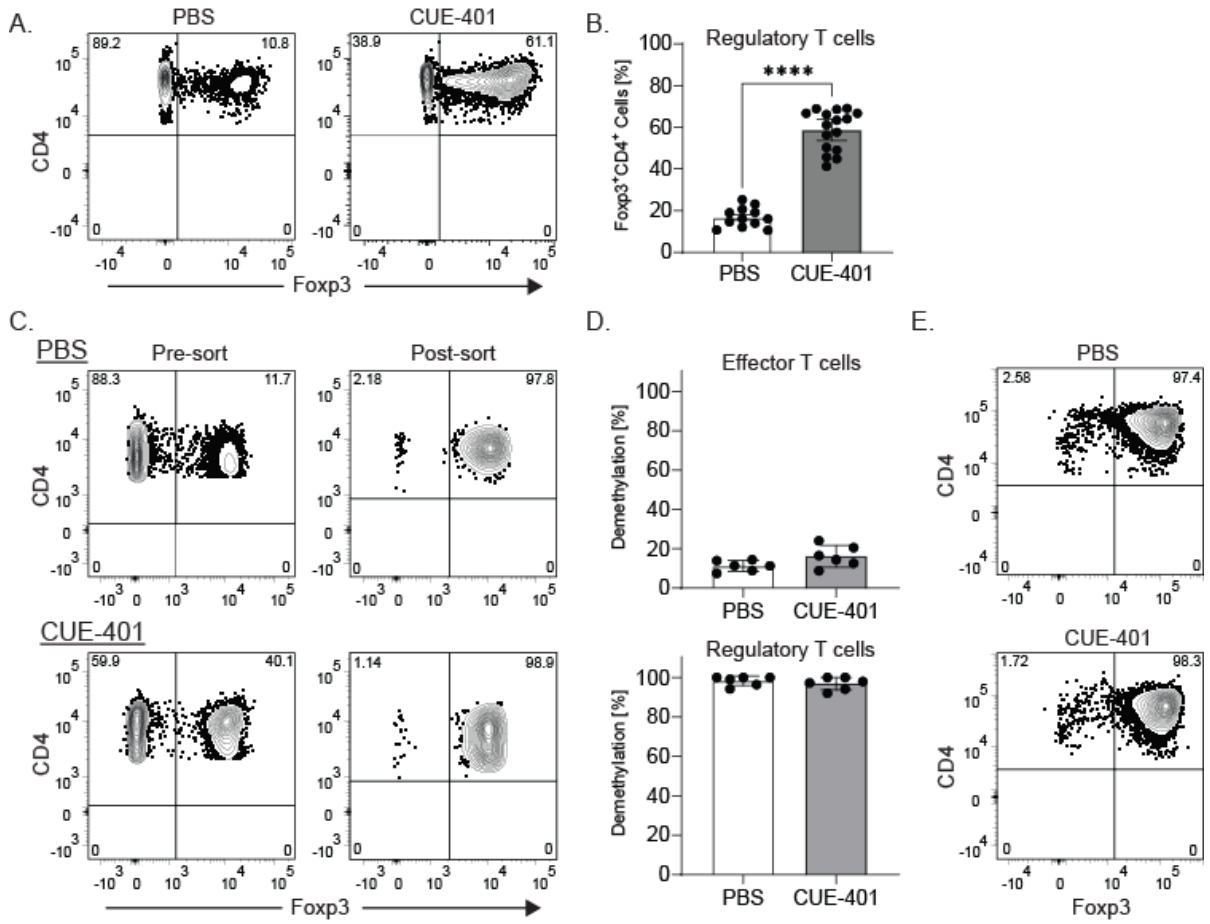

Fig. 3. CUE-401 treatment increases proportions of stable Foxp3+ Tregs in vivo

(**A**) Flow cytometric analysis showing percentages of $CD4^+$ gated cells expressing Foxp3 six days after treatment of BALB/c mice. (**B**) Combined data for the percentages of $CD4^+Foxp3^+$ Tregs in PBS and CUE-401 treated mice. (**C**) Flow cytometric analysis of $CD4^+Foxp3^+$ expression prior to and after performing FACS to purify $CD4^+Foxp3^+GFP^+$ Tregs. (**D**) Results of qPCR quantifying the relative percentage of DNA demethylation at key CpG sites within the Treg-specific demethylated region (TSDR) of the *Foxp3* locus of $CD4^+$Foxp3.eGFP$^-$ and $CD4^+$Foxp3.eGFP$^+$ cells sorted from PBS and CUE-401 treated mice. (**E**) Representative flow cytometric plots showing Foxp3 expression of purified T cells from PBS and CUE-401 treated mice after 6 days of restimulation in vitro in the absence of cytokines. For all graphs, controls were PBS treated age-matched mice. Data in (A-B) was generated from spleens of 2-5 mice in 7 independent experiments. Plots in (C) show the average proportion of $Foxp3^+$ T cells pre and post sorting from 8 mice in 2 independent experiments. Bars represent the median +/- 95% C.I. TSDR

analysis in (D) includes 12 mice from 2 independent experiments. Female mice methylation status was normalized for methylation state on both x chromosomes. *P* values were calculated utilizing the Mann-Whitney *U* test. ****$p < 0.001$.

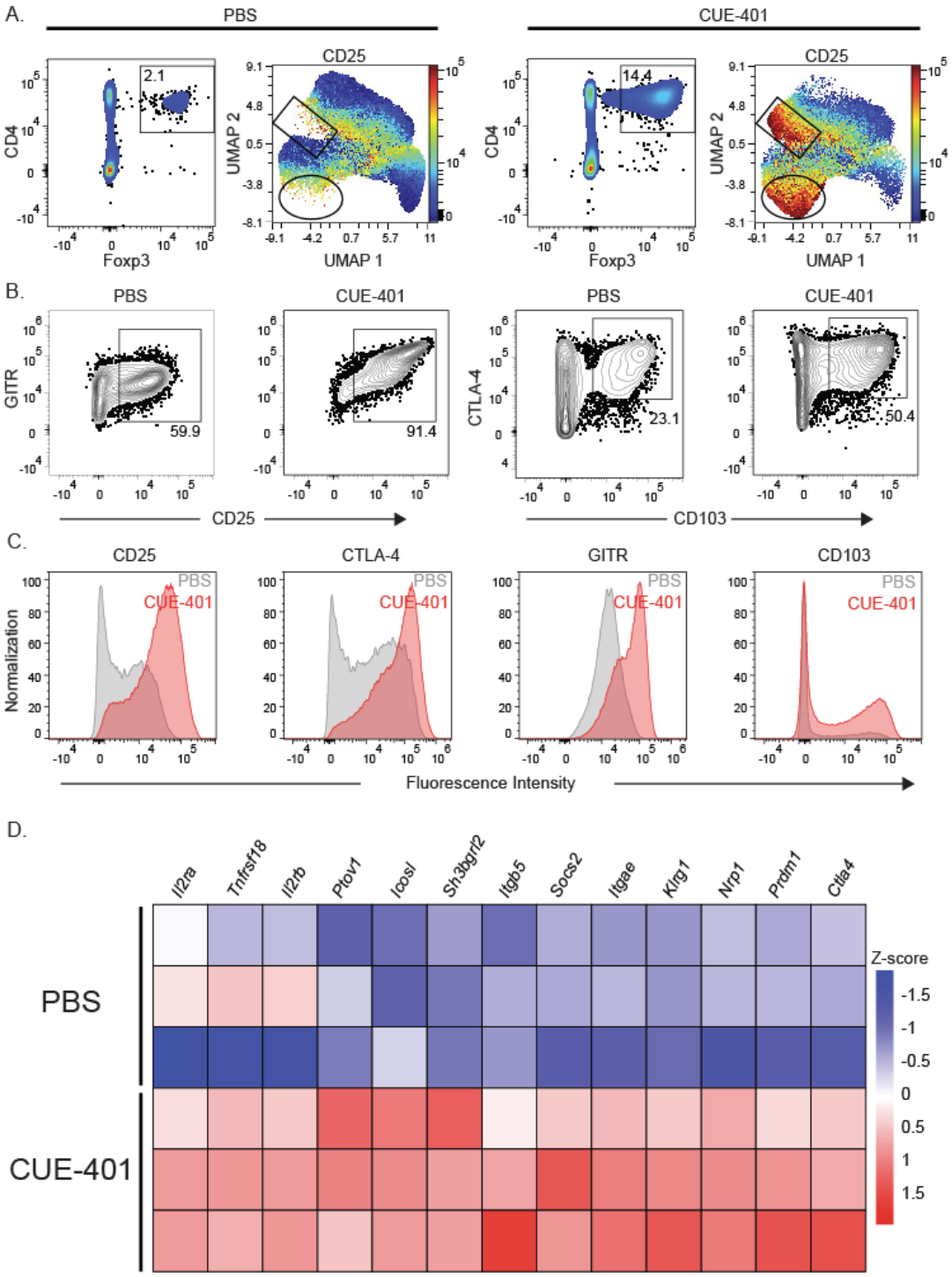

643 **Fig. 4. CUE-401 increases expression of transcripts and proteins associated with Treg activation.**
644 (**A**). Flow cytometric analysis shows the percentage of $CD4^+Foxp3^+$ expressing cells following treatment
645 of mice with PBS or CUE-401. $CD4^+Foxp3^+$ Tregs were identified, and UMAP projections were
646 generated using OMIQ software to cluster cells based on protein expression. The feature plot shows
647 CD25 expression within the $Foxp3^+$ populations. (**B**). Cells were gated on the $CD4^+Foxp3^+$ populations to
648 assess surface expression of GITR, CD25, CTLA-4 and CD103. (**C**). Histograms display the expression
649 of GITR, CD25, CTLA-4, and CD103 within the Treg compartment of PBS-treated controls compared to
650 CUE-401–treated mice. (**D**). Heatmap from bulk RNA sequencing of sorted Tregs, highlighting
651 differentially expressed genes between PBS and CUE-401 treated mice. Genes included had a $\log_2$ fold
652 change > 2 and adjusted p-value < 0.05, using the Benjamini–Hochberg correction to control false
653 discovery rate (FDR). For all flow cytometry plots, data are representative of individual spleens from a
654 single experiment with 3 mice per treatment group. PBS-treated, age-matched mice served as controls in
655 all analyses.

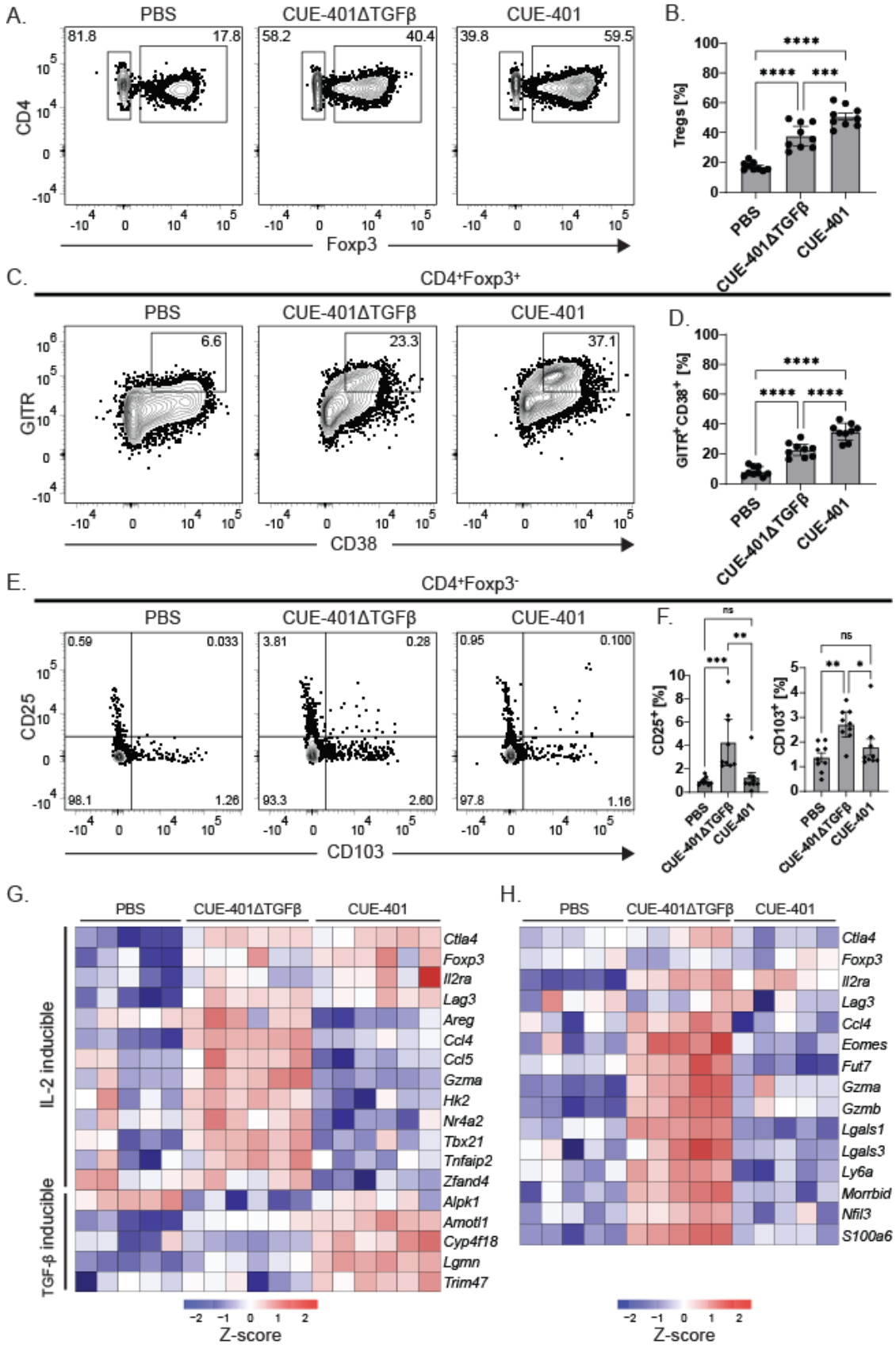
A.
PBS
CUE-401ΔTGFβ
CUE-401
81.8
17.8
58.2
40.4
39.8
59.5
CD4
Foxp3
B.
Tregs [%]
PBS
CUE-401ΔTGFβ
CUE-401
C.
CD4+Foxp3+
6.6
23.3
37.1
GITR
CD38
D.
GITR+CD38+ [%]
E.
CD4+Foxp3-
0.59
0.033
98.1
1.26
3.81
0.28
93.3
2.60
0.95
0.100
97.8
1.16
CD25
CD103
F.
CD25+ [%]
CD103+ [%]
ns
G.
H.
IL-2 inducible
TGF-β inducible
Ctla4
Foxp3
Il2ra
Lag3
Areg
Ccl4
Ccl5
Gzma
Hk2
Nr4a2
Tbx21
Tnfaip2
Zfand4
Alpk1
Amotl1
Cyp4f18
Lgmn
Trim47
Ccl4
Eomes
Fut7
Gzmb
Lgals1
Lgals3
Ly6a
Morrbid
Nfil3
S100a6
Z-score

656

657 **Fig. 5. The combined effects of IL-2 and TGF-β3 in CUE-401 differ from IL-2 treatment alone.**
658 (**A**). Representative flow cytometric analysis showing the percentage of $CD4^+$ gated cells expressing
659 Foxp3 six days after treatment with PBS (left), CUE-401ΔTGF-β3 (middle), or CUE-401 (right) in vivo.
660 (**B**). Combined data showing the percentages of $CD4^+Foxp3^+$ Tregs in PBS, CUE-401ΔTGF-β3, or CUE-
661 401 treated mice. (**C**). Representative flow cytometric analysis comparing GITR by CD38 expression in
662 $CD4^+Foxp3^+$ Tregs following the indicated treatments. (**D**). Combined data showing the percentage of
663 $GITR^+CD38^+$ Tregs following PBS, CUE-401ΔTGF-β3, or CUE-401 treatment. (**E**). Representative flow
664 cytometric analysis comparing CD25 by CD103 of $CD4^+Foxp3^-$ gated cells. (**F**). Combined data showing
665 the percentage of $CD25^+CD4^+Foxp3^-$ cells and $CD103^+CD4^+Foxp3^-$ cells six days after treatment. Data
666 shown are representative of two independent experiments (N = 9 per group). Bars represent the median ±
667 95% confidence interval. (**G**, **H**). Heatmaps of gene expression profiles in sorted $CD4^+Foxp3.eGFP^+$
668 Treg cells or $CD4^+Foxp3.eGFP^-$ Tconv cells, derived from a subset of control or treated mice (N = 2,3 per
669 group, respectively). *P* values for flow results were determined utilizing an ordinary one-way ANOVA
670 with Tukey's multiple comparisons test with $*p = 0.0332$, $**p = 0.0021$, $***\ p = 0.0002$, and $****p <$
671 0.0001.
672
673

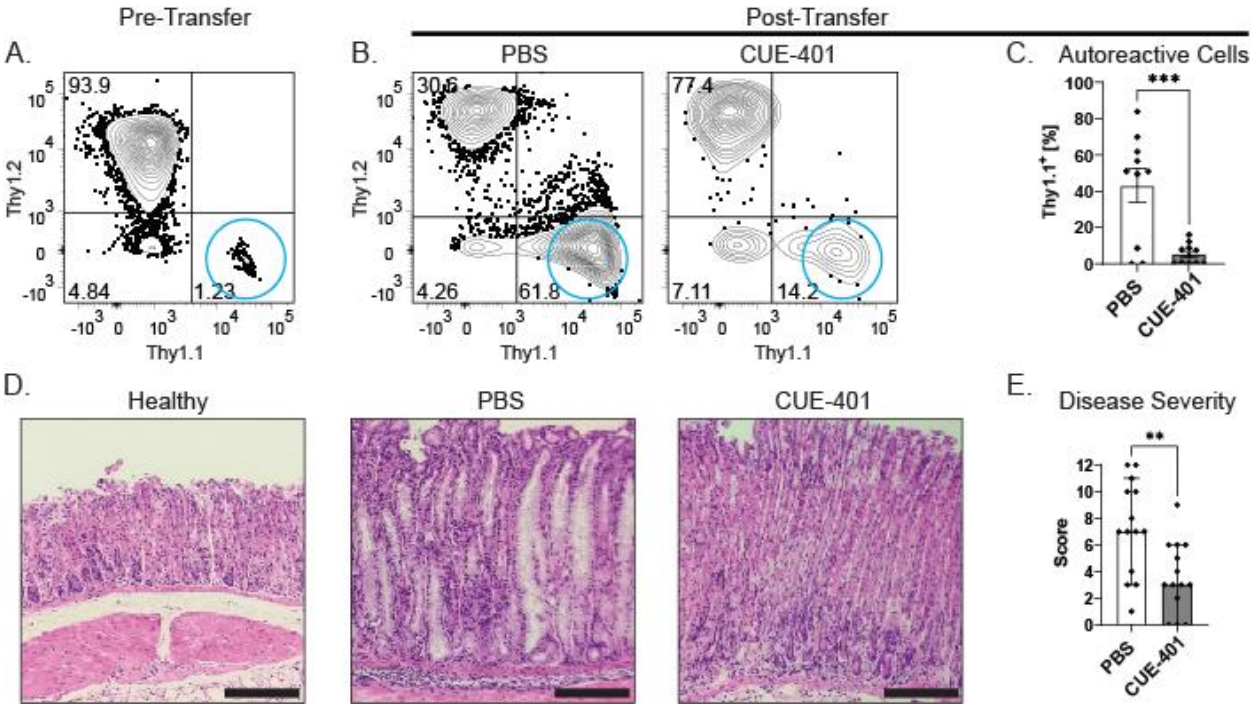

674

675 **Fig. 6. CUE-401 treatment inhibits Teff responses and decreases autoimmune disease severity.**

676 (**A**). Flow cytometric analysis of Thy1.2^{+}CD4^{+} splenocytes and autoreactive Thy1.1^{+}CD4^{+} splenocytes

677 prior to injection into BALB/c *nu/nu* mice. (**B**). Flow cytometric analysis of Thy1.1 and Thy1.2

678 expression in CD4^{+} T cells from stomachs of BALB/c *nu/nu* mice ~62 days after transfer. (**C**) Combined

679 analysis of Thy1.1 expressing autoreactive cells in the gastric mucosa of nude mice ~62 days after

680 transfer and subsequent treatment with PBS or CUE-401. Quantified data are presented as mean ± SEM.

681 Experiments were conducted independently three times, with 2–5 mice per group per experiment. (**D**).

682 Representative images from four independent experiments, comparing tissues from healthy untreated

683 BALB/c mice, PBS-treated BALB/c *nu/nu* controls, and CUE-401–treated BALB/c *nu/nu* mice. (**E**).

684 Histological disease scores were determined based on multiple pathological features, including

685 inflammation, glandular atrophy, and epithelial hyperplasia. The final score represents the combined

686 values from these categories. Graph bars represent the median +/- 95% C.I. Experiments contained 3-5

687 aged matched female mice. *P*-values were determined utilizing either Unpaired Student's T test (C) or

688 Mann-Whitney *U* test (D) with $^{**}p = 0.0040$ and $^{***}p = 0.0005$. Scale bars in micrographs represent 180

689 μM.

690

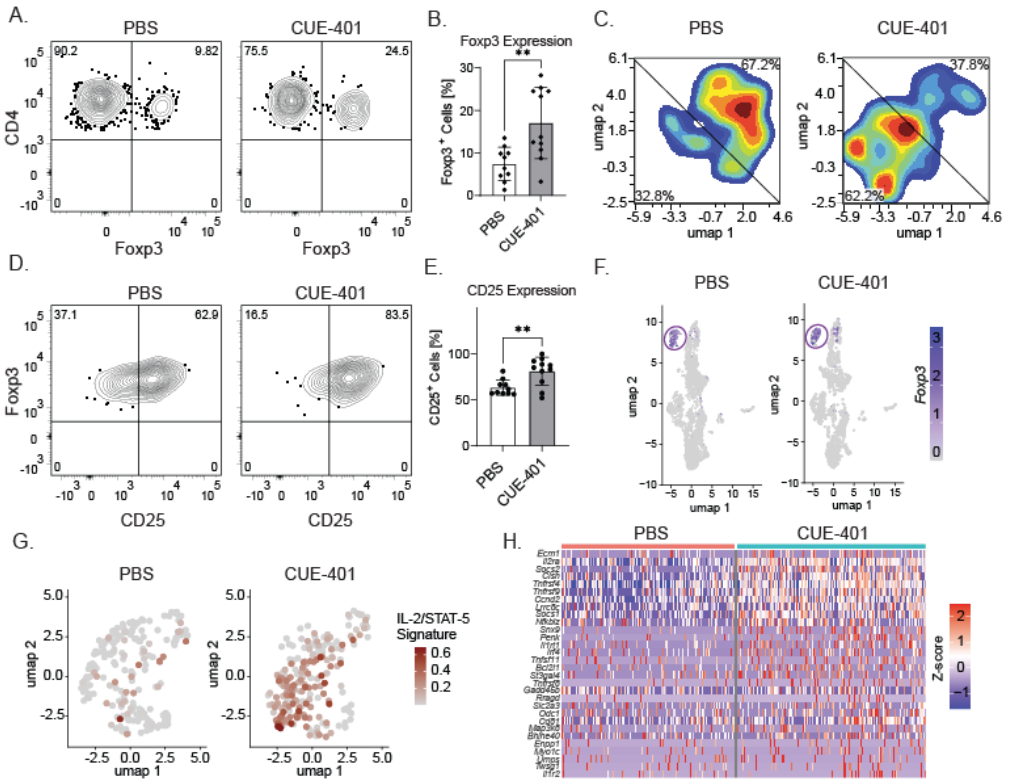

691

692 **Fig. 7. CUE-401 induces activated Tregs with a distinct transcriptional program.**

693 (**A**). Representative flow cytometric analysis of CD4 gated Foxp3^{+} cells in PBS and CUE-401 treated

694 BALB/c nude mice 7 days after splenocyte transfer. (**B**). Cumulative data showing the percentages of

695 CD4^{+}Foxp3^{+} Tregs in PBS and CUE-401 treated mice 6 days after a single treatment. (**C**). CD4^{+}Foxp3^{+}

696 Tregs were identified in each treatment condition, and UMAP projections generated distinct clusters of

697 cells based on protein expression. (**D**). Representative flow cytometric analysis of CD4^{+}Foxp3^{+} gated,

698 CD25 expressing cells. (**E**). Combined data showing the percentages of CD25 expressing Tregs in PBS

699 and CUE-401 treated mice. (**F**). Single cell RNA sequencing clustering analysis of T cells. T cell

700 populations were subset and Foxp3 expression identified the Treg populations in PBS and CUE-401

701 treated mice. (**G**). Foxp3 expressing T cells were re-clustered and signatures were generated based on IL-

702 2/STAT5 signaling transcripts that were identified through gene set enrichment analysis

703 (**H**). Heatmap that highlights differentially expressed genes in single Foxp3^{+} cells between PBS and CUE-

704 401 treatment. Differential expression analysis between CUE-401 and PBS Tregs used the Wilcoxon

705 rank-sum test implemented in Seurat. P-values were adjusted for multiple comparisons using the
706 Benjamini–Hochberg method to control false discovery rate (FDR). Representative images in (A) from 3
707 independent experiments with 3-5 age matched female mice per experiment. *P*-values were determined
708 utilizing Mann-Whitney *U* test with $p < 0.05$ as significant for the flow cytometry analyses. Single cell
709 analysis in (F-H) generated cells of 8 total mice in 2 independent experiments (4 treated and 4 untreated).
710

711 **Acknowledgments:**

712 We thank Saint Louis University Flow Cytometry Core (Joy Eslick, and Jacqueline Spencer) and the
713 Advanced Research Histology Facility (Caroline Murphy, Vasiliki Grammatopoulou) for assistance with
714 data collection. We thank Saint Louis University Genomics and Bioinformatics Core Facility (Dr.
715 Michelle Brennan) for assistance with processing and analysis of single cell and bulk RNA sequencing.
716 We thank Saint Louis University Department of Comparative Medicine (Lisa Tempel, Tawanika
717 Williams, Kelsey Ernst) for assistance in animal care and handling

718

719 **Funding:**

720 This work was funded in part by a sponsored research agreement between CUE Biopharma and Saint
721 Louis University.

722

723 **Author contributions:**

724 Conceptualization: NMJ, RS, NMG, SNQ, AS, CAP, SGH, EF, RJD

725 Methodology: NMJ, NMG, SNQ, RJD, SL, EC, KY, EN

726 Investigation: NMJ

727 Visualization: NMJ, KF, JAC, RJD

728 Formal Analysis: NMJ, NY, CAP, SGH, KF, EF

729 Software: SGH, KF

730 Funding acquisition: AS, NMG, SNQ, RJD

731 Writing – original draft: NMJ, JAC, RJD

732 Writing – review & editing: NMJ, JAC, NMG, SNQ, RJD

733 All authors approved the final manuscript.

734

735 **Competing interests:** AS, SL, NMG, SNQ, RS, KY, EN, and EC are employees of CUE Biopharma. All

736 other authors declare that they have no competing interests.

737

738 **Data and materials availability:** All data necessary to understand and evaluate the conclusions of the

739 paper are provided in the manuscript and supplementary materials. The CUE-401 biologic can be

740 available upon request under a material transfer agreement with CUE Biopharma. Sequencing

741 data will be made publicly available upon acceptance of this publication.

742

743

744

745

746

747

748

749

750 **References:**

751 1. S. Sakaguchi, N. Sakaguchi, M. Asano, M. Itoh, M. Toda, Immunologic self-tolerance maintained by
752 activated T cells expressing IL-2 receptor alpha-chains (CD25). Breakdown of a single mechanism of self-
753 tolerance causes various autoimmune diseases. *J Immunol* **155**, 1151-1164 (1995).
754 2. L. Wang *et al.*, Regulatory T cells in homeostasis and disease: molecular mechanisms and therapeutic
755 potential. *Signal Transduct Target Ther* **10**, 345 (2025).
756 3. C. L. Bennett *et al.*, The immune dysregulation, polyendocrinopathy, enteropathy, X-linked syndrome
757 (IPEX) is caused by mutations of FOXP3. *Nat Genet* **27**, 20-21 (2001).
758 4. S. Hori, T. Nomura, S. Sakaguchi, Control of regulatory T cell development by the transcription factor
759 Foxp3. *Science* **299**, 1057-1061 (2003).
760 5. R. Khattri, T. Cox, S. A. Yasayko, F. Ramsdell, An essential role for Scurfin in CD4+CD25+ T regulatory
761 cells. *Nat Immunol* **4**, 337-342 (2003).
762 6. J. D. Fontenot, M. A. Gavin, A. Y. Rudensky, Foxp3 programs the development and function of
763 CD4+CD25+ regulatory T cells. *Nat Immunol* **4**, 330-336 (2003).
764 7. E. M. Shevach, A. M. Thornton, tTregs, pTregs, and iTregs: similarities and differences. *Immunol Rev* **259**,
765 88-102 (2014).
766 8. A. Jones, D. Hawiger, Peripherally Induced Regulatory T Cells: Recruited Protectors of the Central
767 Nervous System against Autoimmune Neuroinflammation. *Front Immunol* **8**, 532 (2017).
768 9. T. S. Davidson, R. J. DiPaolo, J. Andersson, E. M. Shevach, Cutting Edge: IL-2 is essential for TGF-beta-
769 mediated induction of Foxp3+ T regulatory cells. *J Immunol* **178**, 4022-4026 (2007).
770 10. W. Chen *et al.*, Conversion of peripheral CD4+CD25- naive T cells to CD4+CD25+ regulatory T cells by
771 TGF-beta induction of transcription factor Foxp3. *J Exp Med* **198**, 1875-1886 (2003).
772 11. T. L. Nguyen, N. T. Makhlouf, B. A. Anthony, R. M. Teague, R. J. DiPaolo, In vitro induced regulatory T
773 cells are unique from endogenous regulatory T cells and effective at suppressing late stages of ongoing
774 autoimmunity. *PLoS One* **9**, e104698 (2014).
775 12. S. E. Weber *et al.*, Adaptive islet-specific regulatory CD4 T cells control autoimmune diabetes and mediate
776 the disappearance of pathogenic Th1 cells in vivo. *J Immunol* **176**, 4730-4739 (2006).
777 13. R. J. DiPaolo *et al.*, Autoantigen-specific TGFbeta-induced Foxp3+ regulatory T cells prevent
778 autoimmunity by inhibiting dendritic cells from activating autoreactive T cells. *J Immunol* **179**, 4685-4693
779 (2007).
780 14. S. G. Zheng *et al.*, CD4+ and CD8+ regulatory T cells generated ex vivo with IL-2 and TGF-beta suppress
781 a stimulatory graft-versus-host disease with a lupus-like syndrome. *J Immunol* **172**, 1531-1539 (2004).
782 15. M. E. Raeber, D. Sahin, U. Karakus, O. Boyman, A systematic review of interleukin-2-based
783 immunotherapies in clinical trials for cancer and autoimmune diseases. *EBioMedicine* **90**, 104539 (2023).
784 16. R. Zhang *et al.*, Low-dose IL-2 therapy in autoimmune diseases: An update review. *Int Rev Immunol* **43**,
785 113-137 (2024).
786 17. L. Khoryati *et al.*, An IL-2 mutein engineered to promote expansion of regulatory T cells arrests ongoing
787 autoimmunity in mice. *Sci Immunol* **5**, (2020).
788 18. S. N. Quayle *et al.*, CUE-101, a Novel E7-pHLA-IL2-Fc Fusion Protein, Enhances Tumor Antigen-
789 Specific T-Cell Activation for the Treatment of HPV16-Driven Malignancies. *Clin Cancer Res* **26**, 1953-
790 1964 (2020).
791 19. D. J. Stauber, E. W. Debler, P. A. Horton, K. A. Smith, I. A. Wilson, Crystal structure of the IL-2 signaling
792 complex: paradigm for a heterotrimeric cytokine receptor. *Proc Natl Acad Sci U S A* **103**, 2788-2793
793 (2006).
794 20. K. M. Heaton, G. Ju, E. A. Grimm, Human interleukin 2 analogues that preferentially bind the
795 intermediate-affinity interleukin 2 receptor lead to reduced secondary cytokine secretion: implications for
796 the use of these interleukin 2 analogues in cancer immunotherapy. *Cancer Res* **53**, 2597-2602 (1993).
797 21. T. R. Mosmann *et al.*, Species-specificity of T cell stimulating activities of IL 2 and BSF-1 (IL 4):
798 comparison of normal and recombinant, mouse and human IL 2 and BSF-1 (IL 4). *J Immunol* **138**, 1813-
799 1816 (1987).
800 22. K. Abnaof *et al.*, TGF-beta stimulation in human and murine cells reveals commonly affected biological
801 processes and pathways at transcription level. *BMC Syst Biol* **8**, 55 (2014).
802 23. J. E. Zuniga *et al.*, Assembly of TbetaRI:TbetaRII:TGFbeta ternary complex in vitro with receptor
803 extracellular domains is cooperative and isoform-dependent. *J Mol Biol* **354**, 1052-1068 (2005).

24. J. Groppe *et al.*, Cooperative assembly of TGF-beta superfamily signaling complexes is mediated by two disparate mechanisms and distinct modes of receptor binding. *Mol Cell* **29**, 157-168 (2008).
25. X. Li, Y. Liang, M. LeBlanc, C. Benner, Y. Zheng, Function of a Foxp3 cis-element in protecting regulatory T cell identity. *Cell* **158**, 734-748 (2014).
26. A. S. Wegrzyn, A. E. Kedzierska, A. Obojski, Identification and classification of distinct surface markers of T regulatory cells. *Front Immunol* **13**, 1055805 (2022).
27. C. Gootjes, J. J. Zwaginga, B. O. Roep, T. Nikolic, Defining Human Regulatory T Cells beyond FOXP3: The Need to Combine Phenotype with Function. *Cells* **13**, (2024).
28. S. Dikiy, A. Y. Rudensky, Principles of regulatory T cell function. *Immunity* **56**, 240-255 (2023).
29. J. D. Fontenot, J. P. Rasmussen, M. A. Gavin, A. Y. Rudensky, A function for interleukin 2 in Foxp3-expressing regulatory T cells. *Nat Immunol* **6**, 1142-1151 (2005).
30. A. Arvey *et al.*, Inflammation-induced repression of chromatin bound by the transcription factor Foxp3 in regulatory T cells. *Nat Immunol* **15**, 580-587 (2014).
31. J. A. Hill *et al.*, Foxp3 transcription-factor-dependent and -independent regulation of the regulatory T cell transcriptional signature. *Immunity* **27**, 786-800 (2007).
32. N. Sugimoto *et al.*, Foxp3-dependent and -independent molecules specific for CD25+CD4+ natural regulatory T cells revealed by DNA microarray analysis. *Int Immunol* **18**, 1197-1209 (2006).
33. M. Ahn, J. Dostal, P. Hegde, D. J. Lee, CTLA-4 expression on tregs is needed for suppression of autoimmune uveitis. *Sci Rep* **15**, 17745 (2025).
34. M. G. Petrillo *et al.*, GITR+ regulatory T cells in the treatment of autoimmune diseases. *Autoimmun Rev* **14**, 117-126 (2015).
35. S. Tagkareli *et al.*, CD103 integrin identifies a high IL-10-producing FoxP3(+) regulatory T-cell population suppressing allergic airway inflammation. *Allergy* **77**, 1150-1164 (2022).
36. K. E. Earle *et al.*, In vitro expanded human CD4+CD25+ regulatory T cells suppress effector T cell proliferation. *Clin Immunol* **115**, 3-9 (2005).
37. R. S. McHugh, E. M. Shevach, D. H. Margulies, K. Natarajan, A T cell receptor transgenic model of severe, spontaneous organ-specific autoimmunity. *Eur J Immunol* **31**, 2094-2103 (2001).
38. R. J. DiPaolo, D. D. Glass, K. E. Bijwaard, E. M. Shevach, CD4+CD25+ T cells prevent the development of organ-specific autoimmune disease by inhibiting the differentiation of autoreactive effector T cells. *J Immunol* **175**, 7135-7142 (2005).
39. S. Gaggero *et al.*, IL-2 is inactivated by the acidic pH environment of tumors enabling engineering of a pH-selective mutein. *Sci Immunol* **7**, eade5686 (2022).
40. W. J. Leonard, J. X. Lin, Strategies to therapeutically modulate cytokine action. *Nat Rev Drug Discov* **22**, 827-854 (2023).
41. D. A. Horwitz *et al.*, Nanoparticles loaded with IL-2 and TGF-beta promote transplantation tolerance to alloantigen. *Front Immunol* **15**, 1429335 (2024).
42. W. Lin *et al.*, Regulatory T cell development in the absence of functional Foxp3. *Nat Immunol* **8**, 359-368 (2007).
43. F. Alderuccio, B. H. Toh, P. A. Gleeson, I. R. van Driel, A novel method for isolating mononuclear cells from the stomachs of mice with experimental autoimmune gastritis. *Autoimmunity* **21**, 215-221 (1995).
44. Y. Hao *et al.*, Dictionary learning for integrative, multimodal and scalable single-cell analysis. *Nat Biotechnol* **42**, 293-304 (2024).
45. D. Haribhai *et al.*, Regulatory T cells dynamically control the primary immune response to foreign antigen. *J Immunol* **178**, 2961-2972 (2007).
46. Q. Sun *et al.*, Facile induction of immune tolerance by an interleukin-2-TGFbeta surrogate agonist. *Nature*, (2026).